Measurement of Dijet Angular Distributions and Search for Quark Compositeness

B. Abbott,[28] M. Abolins,[25] B.S. Acharya,[43] I. Adam,[12] D.L. Adams,[37] M. Adams,[17] S. Ahn,[14] H. Aihara,[22] G.A. Alves,[10] E. Amidi,[29] N. Amos,[24] E.W. Anderson,[19] R. Astur,[42] M.M. Baarmand,[42] A. Baden,[23] V. Balamurali,[32] J. Balderston,[16] B. Baldin,[14] S. Banerjee,[43] J. Bantly,[5] J.F. Bartlett,[14] K. Bazizi,[39] A. Belyaev,[26] S.B. Beri,[34] I. Bertram,[31] V.A. Bezzubov,[35] P.C. Bhat,[14] V. Bhatnagar,[34] M. Bhattacharjee,[13] N. Biswas,[32] G. Blazey,[30] S. Blessing,[15] P. Bloom,[7] A. Boehnlein,[14] N.I. Bojko,[35] F. Borcherding,[14] C. Boswell,[9] A. Brandt,[14] R. Brock,[25] A. Bross,[14] D. Buchholz,[31] V.S. Burtovoi,[35] J.M. Butler,[3] W. Carvalho,[10] D. Casey,[39] Z. Casilum,[42] H. Castilla-Valdez,[11] D. Chakraborty,[42] S.-M. Chang,[29] S.V. Chekulaev,[35] L.-P. Chen,[22] W. Chen,[42] S. Choi,[41] S. Chopra,[24] B.C. Choudhary,[9] J.H. Christenson,[14] M. Chung,[17] D. Claes,[27] A.R. Clark,[22] W.G. Cobau,[23] J. Cochran,[9] W.E. Cooper,[14] C. Cretsinger,[39] D. Cullen-Vidal,[5] M.A.C. Cummings,[16] D. Cutts,[5] O.I. Dahl,[22] K. Davis,[2] K. De,[44] K. Del Signore,[24] M. Demarteau,[14] D. Denisov,[14] S.P. Denisov,[35] H.T. Diehl,[14] M. Diesburg,[14] G. Di Loreto,[25] P. Draper,[44] Y. Ducros,[40] L.V. Dudko,[26] S.R. Dugad,[43] D. Edmunds,[25] J. Ellison,[9] V.D. Elvira,[42] R. Engelmann,[42] S. Eno,[23] G. Eppley,[37] P. Ermolov,[26] O.V. Eroshin,[35] V.N. Evdokimov,[35] T. Fahland,[8] M. Fatyga,[4] M.K. Fatyga,[39] J. Featherly,[4] S. Feher,[14] D. Fein,[2] T. Ferbel,[39] G. Finocchiaro,[42] H.E. Fisk,[14] Y. Fisyak,[7] E. Flattum,[14] G.E. Forden,[2] M. Fortner,[30] K.C. Frame,[25] S. Fuess,[14] E. Gallas,[44] A.N. Galyaev,[35] P. Gartung,[9] T.L. Geld,[25] R.J. Genik II,[25] K. Genser,[14] C.E. Gerber,[14] B. Gibbard,[4] S. Glenn,[7] B. Gobbi,[31] M. Goforth,[15] A. Goldschmidt,[22] B. Gómez,[1] G. Gómez,[23] P.I. Goncharov,[35] J.L. González Solís,[11] H. Gordon,[4] L.T. Goss,[45] K. Gounder,[9] A. Goussiou,[42] N. Graf,[4] P.D. Grannis,[42] D.R. Green,[14] J. Green,[30] H. Greenlee,[14] G. Grim,[7] S. Grinstein,[6] N. Grossman,[14] P. Grudberg,[22] S. Grünendahl,[39] G. Guglielmo,[33] J.A. Guida,[2] J.M. Guida,[5] A. Gupta,[43] S.N. Gurzhiev,[35] P. Gutierrez,[33] Y.E. Gutnikov,[35] N.J. Hadley,[23] H. Haggerty,[14] S. Hagopian,[15] V. Hagopian,[15] K.S. Hahn,[39] R.E. Hall,[8] P. Hanlet,[29] S. Hansen,[14] J.M. Hauptman,[19] D. Hedin,[30] A.P. Heinson,[9] U. Heintz,[14] R. Hernández-Montoya,[11] T. Heuring,[15] R. Hirosky,[15] J.D. Hobbs,[14] B. Hoeneisen,[1,†] J.S. Hoftun,[5] F. Hsieh,[24] Ting Hu,[42] Tong Hu,[18] T. Huehn,[9] A.S. Ito,[14] E. James,[2] J. Jaques,[32] S.A. Jerger,[25] R. Jesik,[18] J.Z.-Y. Jiang,[42] T. Joffe-Minor,[31] K. Johns,[2] M. Johnson,[14] A. Jonckheere,[14] M. Jones,[16] H. Jöstlein,[14] S.Y. Jun,[31] C.K. Jung,[42] S. Kahn,[4] G. Kalbfleisch,[33] J.S. Kang,[20] R. Kehoe,[32] M.L. Kelly,[32] C.L. Kim,[20] S.K. Kim,[41] A. Klatchko,[15] B. Klima,[14] C. Klopfenstein,[7] V.I. Klyukhin,[35] V.I. Kochetkov,[35] J.M. Kohli,[34] D. Koltick,[36] A.V. Kostritskiy,[35] J. Kotcher,[4] A.V. Kotwal,[12] J. Kourlas,[28] A.V. Kozelov,[35] E.A. Kozlovski,[35] J. Krane,[27] M.R. Krishnaswamy,[43] S. Krzywdzinski,[14] S. Kunori,[23] S. Lami,[42] H. Lan,[14,*] R. Lander,[7] F. Landry,[25] G. Landsberg,[14] B. Lauer,[19] A. Leflat,[26] H. Li,[42] J. Li,[44] Q.Z. Li-Demarteau,[14] J.G.R. Lima,[38] D. Lincoln,[24] S.L. Linn,[15] J. Linnemann,[25] R. Lipton,[14] Q. Liu,[14,*] Y.C. Liu,[31] F. Lobkowicz,[39] S.C. Loken,[22] S. Lökös,[42] L. Lueking,[14] A.L. Lyon,[23] A.K.A. Maciel,[10] R.J. Madaras,[22] R. Madden,[15] L. Magaña-Mendoza,[11] S. Mani,[7] H.S. Mao,[14,*] R. Markeloff,[30] T. Marshall,[18] M.I. Martin,[14] K.M. Mauritz,[19] B. May,[31] A.A. Mayorov,[35] R. McCarthy,[42] J. McDonald,[15] T. McKibben,[17] J. McKinley,[25]

T. McMahon,[33] H.L. Melanson,[14] M. Merkin,[26] K.W. Merritt,[14] H. Miettinen,[37] A. Mincer,[28] C.S. Mishra,[14] N. Mokhov,[14] N.K. Mondal,[43] H.E. Montgomery,[14] P. Mooney,[1] H. da Motta,[10] C. Murphy,[17] F. Nang,[2] M. Narain,[14] V.S. Narasimham,[43] A. Narayanan,[2] H.A. Neal,[24] J.P. Negret,[1] P. Nemethy,[28] M. Nicola,[10] D. Norman,[45] L. Oesch,[24] V. Oguri,[38] E. Oltman,[22] N. Oshima,[14] D. Owen,[25] P. Padley,[37] M. Pang,[19] A. Para,[14] Y.M. Park,[21] R. Partridge,[5] N. Parua,[43] M. Paterno,[39] J. Perkins,[44] M. Peters,[16] R. Piegaia,[6] H. Piekarz,[15] Y. Pischalnikov,[36] V.M. Podstavkov,[35] B.G. Pope,[25] H.B. Prosper,[15] S. Protopopescu,[4] J. Qian,[24] P.Z. Quintas,[14] R. Raja,[14] S. Rajagopalan,[4] O. Ramirez,[17] L. Rasmussen,[42] S. Reucroft,[29] M. Rijssenbeek,[42] T. Rockwell,[25] N.A. Roe,[22] P. Rubinov,[31] R. Ruchti,[32] J. Rutherfoord,[2] A. Sánchez-Hernández,[11] A. Santoro,[10] L. Sawyer,[44] R.D. Schamberger,[42] H. Schellman,[31] J. Sculli,[28] E. Shabalina,[26] C. Shaffer,[15] H.C. Shankar,[43] R.K. Shivpuri,[13] M. Shupe,[2] H. Singh,[9] J.B. Singh,[34] V. Sirotenko,[30] W. Smart,[14] R.P. Smith,[14] R. Snihur,[31] G.R. Snow,[27] J. Snow,[33] S. Snyder,[4] J. Solomon,[17] P.M. Sood,[34] M. Sosebee,[44] N. Sotnikova,[26] M. Souza,[10] A.L. Spadafora,[22] R.W. Stephens,[44] M.L. Stevenson,[22] D. Stewart,[24] F. Stichelbaut,[42] D.A. Stoianova,[35] D. Stoker,[8] M. Strauss,[33] K. Streets,[28] M. Strovink,[22] A. Sznajder,[10] P. Tamburello,[23] J. Tarazi,[8] M. Tartaglia,[14] T.L.T. Thomas,[31] J. Thompson,[23] T.G. Trippe,[22] P.M. Tuts,[12] N. Varelas,[25] E.W. Varnes,[22] D. Vititoe,[2] A.A. Volkov,[35] A.P. Vorobiev,[35] H.D. Wahl,[15] G. Wang,[15] J. Warchol,[32] G. Watts,[5] M. Wayne,[32] H. Weerts,[25] A. White,[44] J.T. White,[45] J.A. Wightman,[19] S. Willis,[30] S.J. Wimpenny,[9] J.V.D. Wirjawan,[45] J. Womersley,[14] E. Won,[39] D.R. Wood,[29] H. Xu,[5] R. Yamada,[14] P. Yamin,[4] C. Yanagisawa,[42] J. Yang,[28] T. Yasuda,[29] P. Yepes,[37] C. Yoshikawa,[16] S. Youssef,[15] J. Yu,[14] Y. Yu,[41] Z.H. Zhu,[39] D. Zieminska,[18] A. Zieminski,[18] E.G. Zverev,[26] and A. Zylberstejn[40]

(DØ Collaboration)

[1] *Universidad de los Andes, Bogotá, Colombia*
[2] *University of Arizona, Tucson, Arizona 85721*
[3] *Boston University, Boston, Massachusetts 02215*
[4] *Brookhaven National Laboratory, Upton, New York 11973*
[5] *Brown University, Providence, Rhode Island 02912*
[6] *Universidad de Buenos Aires, Buenos Aires, Argentina*
[7] *University of California, Davis, California 95616*
[8] *University of California, Irvine, California 92697*
[9] *University of California, Riverside, California 92521*
[10] *LAFEX, Centro Brasileiro de Pesquisas Físicas, Rio de Janeiro, Brazil*
[11] *CINVESTAV, Mexico City, Mexico*
[12] *Columbia University, New York, New York 10027*
[13] *Delhi University, Delhi, India 110007*
[14] *Fermi National Accelerator Laboratory, Batavia, Illinois 60510*
[15] *Florida State University, Tallahassee, Florida 32306*
[16] *University of Hawaii, Honolulu, Hawaii 96822*
[17] *University of Illinois at Chicago, Chicago, Illinois 60607*
[18] *Indiana University, Bloomington, Indiana 47405*
[19] *Iowa State University, Ames, Iowa 50011*

[20] *Korea University, Seoul, Korea*
[21] *Kyungsung University, Pusan, Korea*
[22] *Lawrence Berkeley National Laboratory and University of California, Berkeley, California 94720*
[23] *University of Maryland, College Park, Maryland 20742*
[24] *University of Michigan, Ann Arbor, Michigan 48109*
[25] *Michigan State University, East Lansing, Michigan 48824*
[26] *Moscow State University, Moscow, Russia*
[27] *University of Nebraska, Lincoln, Nebraska 68588*
[28] *New York University, New York, New York 10003*
[29] *Northeastern University, Boston, Massachusetts 02115*
[30] *Northern Illinois University, DeKalb, Illinois 60115*
[31] *Northwestern University, Evanston, Illinois 60208*
[32] *University of Notre Dame, Notre Dame, Indiana 46556*
[33] *University of Oklahoma, Norman, Oklahoma 73019*
[34] *University of Panjab, Chandigarh 16-00-14, India*
[35] *Institute for High Energy Physics, 142-284 Protvino, Russia*
[36] *Purdue University, West Lafayette, Indiana 47907*
[37] *Rice University, Houston, Texas 77005*
[38] *Universidade do Estado do Rio de Janeiro, Brazil*
[39] *University of Rochester, Rochester, New York 14627*
[40] *CEA, DAPNIA/Service de Physique des Particules, CE-SACLAY, Gif-sur-Yvette, France*
[41] *Seoul National University, Seoul, Korea*
[42] *State University of New York, Stony Brook, New York 11794*
[43] *Tata Institute of Fundamental Research, Colaba, Mumbai 400005, India*
[44] *University of Texas, Arlington, Texas 76019*
[45] *Texas A&M University, College Station, Texas 77843*
(April 4, 2018)

Abstract

We have measured the dijet angular distribution in $\sqrt{s}$=1.8 TeV $p\bar{p}$ collisions using the DØ detector. Order α_s^3 QCD predictions are in good agreement with the data. At 95% confidence the data exclude models of quark compositeness in which the contact interaction scale is below 2 TeV.

Dijet final states in $p\bar{p}$ collisions can be produced through quark-quark, quark-gluon and gluon-gluon interactions. The angular distributions produced by these processes as predicted by theory are similar. Therefore the dijet angular distribution is insensitive to the relative weighting of the individual hard scattering process and thus is insulated from uncertainties in the parton distribution functions (pdf's). Quantum chromodynamics (QCD) parton-parton scattering processes, which are mainly t-channel exchanges, produce dijet angular distributions peaked at small center of mass scattering angles, while many processes containing new physics are more isotropic. Thus, the dijet angular distribution provides an excellent test of QCD and a means of searching for new physics such as quark compositeness.

We have measured the dijet angular distribution with greater precision over a larger dijet invariant mass range and a larger angular range than previous measurements. Next-to-leading order (NLO) QCD predictions are available [1,2] and comparisons can be made between the data and both leading order (LO) and NLO predictions.

The value of the mass scale, Λ, characterizes the strength of the quark substructure binding interactions and the physical size of the composite states. In the regime where $\Lambda \gg \sqrt{\hat{s}}$ is valid, the quarks appear almost pointlike and any quark substructure coupling can be approximated by a four-Fermi interaction. With this approximation, the effective Lagrangian for a flavor diagonal definite chirality current is [3,4]: $\mathcal{L} = A(2\pi/\Lambda^2)(\bar{q}_H\gamma^\mu q_H)(\bar{q}_H\gamma_\mu q_H)$ where $A = \pm 1$, and H= L, R for left or right handed quarks. While this is not the only possible contact interaction, it is the only one for which calculations are currently available. Since the sign of A is a priori undetermined, limits for constructive interference (A=-1) and destructive interference (A=$+1$) are presented. Previously published results from CDF [5] on dijet angular distributions have been compared to the same model in which all quarks are composite, yielding 95% confidence limits $\Lambda^+ > 1.8$ TeV and $\Lambda^- > 1.6$ TeV on the interaction scales.

The DØ detector, described in detail elsewhere [6], measures jets using uranium-liquid argon sampling calorimeters that provide uniform and hermetic coverage over a large range of pseudorapidity ($|\eta| \leq 4$). Typical transverse segmentation is 0.1×0.1 in $\eta \times \phi$, where ϕ is the azimuthal angle.

The data are from the 93 pb^{-1} sample recorded during the 1994-1995 Tevatron run. Events are selected using a multi-level trigger. The first level requires an inelastic collision by demanding the coincidence of two hodoscopes on either side of the interaction region. In the second level, jet candidates are selected using an array of 40 calorimeter trigger towers 0.8×1.6 in $\eta \times \phi$, covering $|\eta| < 4$. Four different trigger criteria are defined, each requiring a single trigger tower above a different transverse energy (E_T) threshold. The final level, an online software trigger, selects events with a jet above a preset threshold. The E_T thresholds at which the triggers are $> 98\%$ efficient for the η coverage used in this analysis are 55, 90, 120 and 175 GeV.

Jets are reconstructed using a fixed cone algorithm with radius $\mathcal{R}$= $\sqrt{\Delta\eta^2 + \Delta\phi^2} = 0.7$. Calorimeter towers with E_T greater than 1.0 GeV are used as seed towers for jet finding [7]. Jet E_T is defined as the sum of the E_T in the towers with $\mathcal{R} < 0.7$ from the seed tower and a new E_T weighted center of the jet is calculated. This process is repeated until the jet center is stable. When one jet overlaps another, they are merged into a single jet if they share more than 50% of the E_T of the lower E_T jet. Otherwise, they are split into two distinct jets.

Jet energy calibration is performed in a multi-step process [8]. First, the electromagnetic energy scale in the central calorimeter is determined by scaling the energies of electrons from Z boson decays so that the corrected Z mass agrees with the value measured at LEP [9]. Next, the jet response of the central calorimeter is measured using momentum conservation in a sample of photon + jet events. After determining the jet response for the central calorimeter as a function of jet energy, the relative η dependent jet response is measured using both photon + jet and dijet events. One jet (photon) is required to be central and the jet response is measured as a function of the η of the other jet. Jets are also corrected for out-of-cone showering losses, underlying event, multiple $p\bar{p}$ interactions, and effects of

TABLE I. The average mass, maximum χ measured, and the number of events after applying all kinematic cuts.

Trigger E_T Threshold (GeV)	Mass Range (GeV/c^2)	Average Mass (GeV/c^2)	$\chi_{\rm max}$	Number of Events
55	260-425	302	20	4621
90	425-475	447	20	1573
120	475-635	524	13	8789
175	>635	700	11	1074

uranium noise.

Quality cuts are required for the two leading E_T jets in each event. These cuts eliminate spurious jets that arise from noisy calorimeter cells, cosmic rays, and accelerator losses. The efficiencies for these cuts are E_T and η dependent and vary between 90% and 97%.

The dijet invariant mass and kinematic variables of an event are defined using the two highest E_T jets. The center of mass scattering angle, θ^*, and the longitudinal boost, $\eta_{\rm boost}$, are expressed in terms of the pseudorapidities of these two jets: $\eta_{\rm boost}=\frac{1}{2}(\eta_1+\eta_2)$ and $\cos\theta^*=\tanh\eta^*$, where $\eta^*=\frac{1}{2}(\eta_1-\eta_2)$. The dominance of spin-1 gluon exchange gives the angular distribution characteristic of Rutherford scattering: $\mathrm{d}N/\mathrm{dcos}\,\theta^* \propto 1/\sin^4(\theta^*/2)$. To facilitate a comparison with theory, the angular distributions are measured as a function of $\chi=e^{2|\eta^*|}=(1+|\cos\theta^*|)/(1-|\cos\theta^*|)$. This definition translates large values of θ^* to small values of χ (e.g. $\theta^*=90^\circ \leftrightarrow \chi=1$). For Rutherford scattering, $\mathrm{d}N/\mathrm{d}\chi$ is independent of χ.

The data are selected using a dijet invariant mass (M) threshold and restricting the kinematic cuts in order to limit the jets to regions of uniform acceptance [10]. The dijet invariant mass is calculated assuming massless jets and using the expression: $M^2=2E_{T1}E_{T2}(\cosh(\eta_1-\eta_2)-\cos(\phi_1-\phi_2))$. Table I shows the average dijet invariant mass, maximum χ measured, and the number of events for each of four mass ranges. Both $|\eta_1|$ and $|\eta_2|$ are required to be less than 3. To maintain uniform acceptance, we also require $|\eta_{\rm boost}|<1.5$.

Table II shows the dijet angular distribution, $(100/N)(\mathrm{d}N/\mathrm{d}\chi)$, in bins of $\Delta\chi=1$ with its statistical error in the four mass bins. The JETRAD program [2] is used to determine the LO and NLO QCD predictions. The jets at NLO are found using the standard [11] jet definition which combines two partons into a single jet if they are both within $\mathcal{R}$=0.7 of their E_T weighted center. We require that two partons also be closer than $\mathcal{R}_{\rm sep}\times 0.7$ with $\mathcal{R}_{\rm sep}$=1.3 [12,13]. Figure 1 shows the dijet angular distributions normalized to unit area compared to three different theoretical predictions. The dashed and solid curves show the LO and NLO predictions for a single choice of renormalization/factorization scale, $\mu=E_T$ of the leading jet. The dotted curve shows the effects of changing the scale to $\mu=E_T/2$ for the NLO predictions. The LO predictions are insensitive to the renormalization scale, so only one scale is shown. With the large value of $\chi_{\rm max}$, the effects of higher order QCD become apparent. The theoretical predictions are clearly sensitive to the order of the calculation and to the renormalization scale. The NLO predictions are seen to be in better agreement

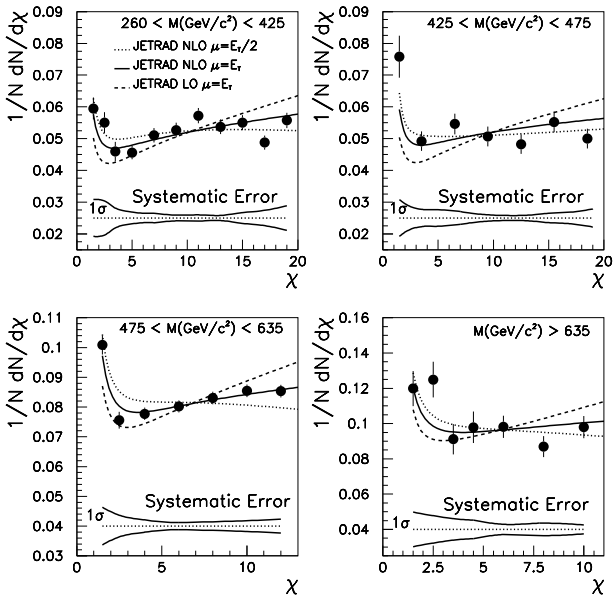

FIG. 1. Dijet angular distributions for DØ data (points) compared to JETRAD for LO (dashed line) and NLO predictions with renormalization/factorization scale μ=E_T(solid line). The data are also compared to JETRAD NLO predictions with μ=$E_T/2$ (dotted line). The errors on the data points are statistical only. The band at the bottom represents the correlated $\pm$ 1 σ systematic uncertainty.

with the data than the LO calculations, especially for large χ.

The dominant source of error on the angular distribution is the uncertainty in the η dependence of the calorimeter energy scale, which is found to be less than 2%. Other systematic uncertainties, including η biases in jet reconstruction, multiple $p\bar{p}$ interactions, η dependent jet quality cut efficiencies, and effects of calorimeter η and E_T smearing are small. Because the data distributions are normalized to unit area, uncertainties in the absolute jet energy scale are minimal. All systematic uncertainties added in quadrature are shown as a band at the bottom of Fig. 1. The effects of a different pdf were examined by replacing the default CTEQ3M [14] with CTEQ2MS [15]. The calculated angular distribution is insensitive to this change.

Because the currently available NLO calculations do not implement the effects of both QCD and quark substructure, possible effects of quark compositeness are determined using a LO simulation [4]. The ratio of the LO predictions with compositeness to the LO predictions with no compositeness is used to scale the NLO calculations. Figure 2 shows the dijet angular distribution for events with $M > 635$ GeV/c^2 compared to theory for different values of the compositeness scale, Λ^+. The largest dijet invariant mass bin is shown because the effects of quark compositeness become more pronounced with increasing dijet invariant mass.

To obtain a compositeness limit, we constructed the variable R_χ, the ratio of the number of events with $\chi < 4$ to the number of events with $4 < \chi < \chi_{\rm max}$. The value $\chi = 4$ is

TABLE II. Dijet angular distribution $(100/N)(\mathrm{d}N/\mathrm{d}\chi)$ with statistical uncertainties for the four mass bins (GeV/c^2).

χ	260< M <425	425< M <475	475< M <635	M >635
1.5	5.94 ± 0.36	7.58 ± 0.69	10.1 ± 0.34	12.0 ± 1.04
2.5	5.50 ± 0.35	4.26 ± 0.52	7.56 ± 0.30	12.5 ± 1.06
3.5	4.59 ± 0.32	4.96 ± 0.57	7.83 ± 0.30	9.11 ± 0.91
4.5	4.57 ± 0.32	5.54 ± 0.59	7.71 ± 0.30	9.79 ± 0.95
5.5	4.56 ± 0.32	5.29 ± 0.58	7.87 ± 0.31	10.1 ± 0.97
6.5	5.10 ± 0.33	6.26 ± 0.64	8.17 ± 0.31	9.58 ± 0.95
7.5	5.10 ± 0.33	4.83 ± 0.56	8.70 ± 0.32	9.30 ± 0.94
8.5	5.61 ± 0.35	4.40 ± 0.53	7.91 ± 0.31	8.08 ± 0.88
9.5	4.93 ± 0.33	5.60 ± 0.60	8.46 ± 0.32	8.96 ± 0.92
10.5	6.04 ± 0.36	5.21 ± 0.58	8.62 ± 0.32	10.6 ± 1.01
11.5	5.40 ± 0.34	4.30 ± 0.53	8.38 ± 0.32	
12.5	5.33 ± 0.34	4.75 ± 0.55	8.69 ± 0.32	
13.5	5.41 ± 0.34	5.43 ± 0.58		
14.5	5.40 ± 0.34	5.69 ± 0.60		
15.5	5.60 ± 0.35	6.18 ± 0.63		
16.5	4.81 ± 0.32	4.70 ± 0.55		
17.5	4.95 ± 0.33	4.83 ± 0.55		
18.5	5.78 ± 0.35	5.01 ± 0.56		
19.5	5.37 ± 0.34	5.17 ± 0.57		

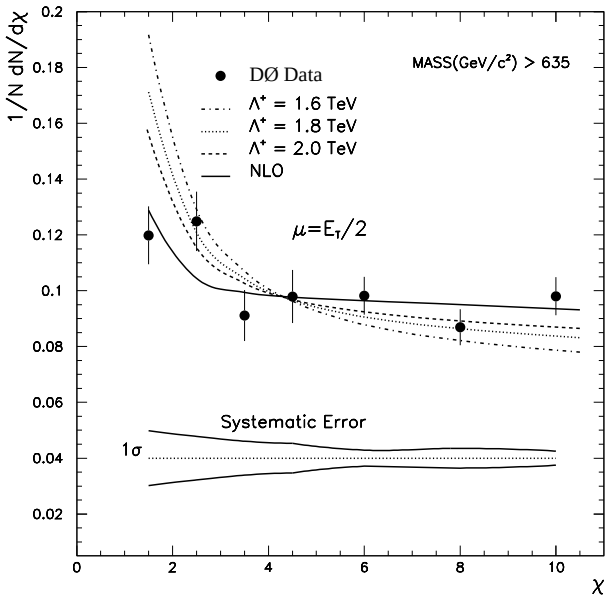

FIG. 2. Data compared to theory for different compositeness scales. See text for how compositeness is calculated for NLO predictions. The errors on the points are statistical and the band represents the correlated $\pm$ 1 σ systematic uncertainty.

chosen to optimize the sensitivity to quark compositeness. Because the angular distribution of jets arising from contact interactions is expected to be more isotropic than that for QCD interactions, contact interactions will produce more events at small χ than QCD and therefore will have a larger value of R_χ. Table III shows the experimental ratio R_χ for the different mass ranges with their statistical and their systematic uncertainties, which are fully correlated in mass. Figure 3 exhibits R_χ as a function of M for two different renormalization scales along with the theoretical predictions for different compositeness scales. Note that the two largest dijet invariant mass bins have a lower $\chi_{\rm max}$ value (Table I), and thus a higher value of R_χ is expected independent of compositeness assumptions. Also shown in Fig. 3 are the χ^2 values for the four degrees of freedom for different values of the compositeness scale. The χ^2 is defined as χ^2=$\sum_{i,j}\delta_i V_{ij}^{-1}\delta_j$, where δ_i is the difference between data and theory in each mass bin i. The covariance matrix, V, is defined as V_{ii}=σ_i^2(stat.)+σ_i^2(syst.), $V_{ij} = \sigma_i$(syst.)σ_j(syst.), for $i \neq j$. For both renormalization scales, the data prefer a model without quark compositeness. The data are better fit with μ=E_T.

We employed a Bayesian technique [16] to obtain a compositeness scale limit from our data, using a Gaussian likelihood function, $P(R_\chi|\xi)$, for R_χ as a function of dijet invariant mass. The compositeness limit depends on the choice of the prior probability distribution, $P(\xi)$. Motivated by the form of the Lagrangian, $P(\xi)$ is assumed to be either flat in ξ=$1/\Lambda^2$ or ξ=$1/\Lambda^4$. Since the dijet angular distribution at NLO is sensitive to the renormalization scale, each renormalization scale is treated as a different theory. The likelihood function has the form $P(R_\chi|\xi) = e^{-\chi^2/2}$. To determine the 95% confidence limit in Λ, a limit in ξ

TABLE III. Values of R_χ with statistical and fully correlated systematic uncertainties.

Mass Range (GeV/c^2)	R_χ	Stat. Error	Syst. Error
260-425	0.191	0.0077	0.015
425-475	0.202	0.0136	0.010
475-635	0.342	0.0085	0.018
> 635	0.506	0.0324	0.028

TABLE IV. The 95% confidence limits for the left-handed contact compositeness scale for different models. The prior probability distribution is assumed to be flat in $1/\Lambda^2$.

Compositeness scale	μ=E_T	μ=$E_T/2$
Λ^+	2.1 TeV	2.3 TeV
Λ^-	2.2 TeV	2.4 TeV
Λ^-_{ud}	2.0 TeV	2.2 TeV

is first calculated by requiring that $Q(\xi) = \int_0^\xi P(R_\chi|\xi')P(\xi')d\xi' = 0.95$ of $Q(\infty)$. The limit in ξ is then transformed back into a limit in Λ. Table IV shows the 95% confidence limits for the compositeness scale obtained for different choices of models using a prior probability distribution which is flat in $1/\Lambda^2$.

If we vary the models to include constructive interference (Λ^-), or require only up and down quarks to be composite (Λ_{ud}), the 95% confidence limits for the compositeness scale change by 0.1 TeV. If the prior probability distribution is assumed to be flat in $1/\Lambda^4$, the 95% confidence limits are reduced by approximately 6%. These limits are valid for either pure left- or right-handed contact interactions. Unlike the earlier measurement [5] using $\chi_{\rm max}$=5, the large χ explored here gives greater sensitivity to compositeness terms with constructive interference than for destructive interference.

In conclusion, we have measured the dijet angular distribution with greater precision over a larger dijet invariant mass range and a larger angular range than previous measurements. The data distributions are in good agreement with NLO QCD predictions. The compositeness limit depends on the choice of the renormalization/factorization scale, the model of compositeness, and the choice of the prior probability function. We have presented compositeness limits for models with left-handed contact interference. With 95% confidence, the interaction scales Λ^+, Λ^-, and Λ^-_{ud} all exceed 2.0 TeV.

We thank R. Harris for the use of his program based on Ref. [4]. We also thank the staffs at Fermilab and collaborating institutions for their contributions to this work, and acknowledge support from the Department of Energy and National Science Foundation (U.S.A.), Commissariat à L'Energie Atomique (France), State Committee for Science and Technology and Ministry for Atomic Energy (Russia), CNPq (Brazil), Departments of Atomic Energy and Science and Education (India), Colciencias (Colombia), CONACyT (Mexico), Ministry of Education and KOSEF (Korea), and CONICET and UBACyT (Argentina).

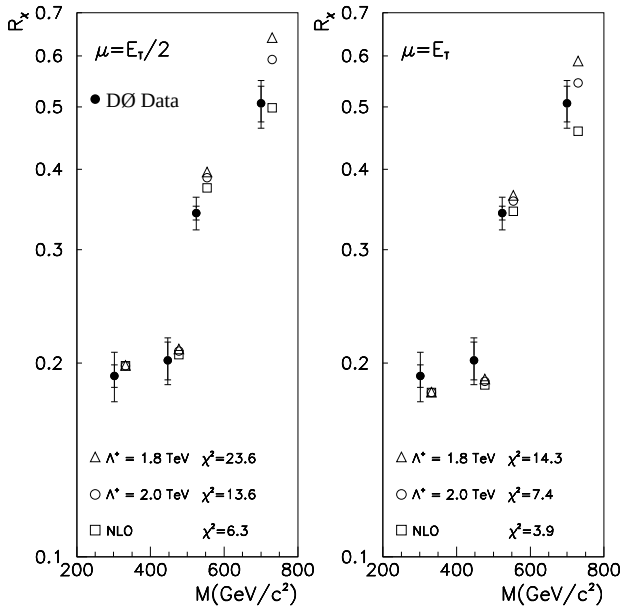

FIG. 3. R_χ as a function of dijet invariant mass for two different renormalization scales. See text for how compositeness is calculated for NLO predictions. The inner error bars are the statistical uncertainties and the outer error bars include the statistical and systematic uncertainties added in quadrature. The χ^2 values for the four degrees of freedom are shown for the different values of the compositeness scale. The DØ data are plotted at the average mass for each mass range. The NLO points are offset in mass to allow the data points to be seen.

REFERENCES

* Visitor from IHEP, Beijing, China.
† Visitor from Univ. San Francisco de Quito, Ecuador.

[1] S.D. Ellis, Z. Kunszt, and D.E. Soper, Phys. Rev. Lett. **64**, 2121 (1990).
[2] W.T. Giele, E.W.N. Glover and D.A. Kosower, Nucl. Phys. B **403**, 633 (1993).
[3] E. Eichten, K. Lane, and M. Peskin, Phys. Rev. Lett. **50**, 811 (1983).
[4] K. Lane, BUHEP-96-8, hep-ph/9605257 (1996).
[5] CDF Collaboration, F. Abe *et al.*, Phys. Rev. Lett. **77**, 5336 (1996). Erratum - ibid. **78**, 4307 (1997).
[6] DØ Collaboration, S. Abachi *et al.*, Nucl. Instrum. and Methods A **338**, 185 (1994).
[7] DØ Collaboration, S. Abachi *et al.*, Phys. Lett. B **357**, 500 (1995).
[8] DØ Collaboration, R. Kehoe, to be published in Proc. 6^{th} International Conf. on Calorimetry in High Energy Physics, Frascati (1996), Fermilab-Conf-96/284-E.
[9] Particle Data Group, "Review of Particle Properties", Phys. Rev D**50**, 1336 (1994).
[10] Mary K. Fatyga, Ph.D. dissertation, University of Rochester, 1996 (unpublished).
[11] J. Huth *et al.*, in proceedings of *Research Directions for the Decade, Snowmass 1990*, edited by E.L. Berger (World Scientific, Singapore, 1992).
[12] S.D. Ellis, Z. Kunzst, and D.E. Soper, Phys. Rev. Lett. **69** ,3615 (1992).
[13] M. Klasen and G. Kramer, hep-ph/9701247 (January 1997).
[14] H.L. Lai *et al.*, (CTEQ Collaboration) Phys. Rev. D **51**, 4763 (1995).
[15] J. Botts, *et al.*, (CTEQ Collaboration) Phys. Lett. B **304**, 159 (1993).
[16] H. Jeffreys, Theory of Probability, Clarendon Press, Oxford (1939, revised 1988).